

Development of optimum cold-formed steel beams for serviceability and ultimate limit states using Big Bang-Big Crunch optimisation

Seyed Mohammad Mojtabaei^{1*}, Jun Ye², Iman Hajirasouliha¹

¹ *Department of Civil and Structural Engineering, The University of Sheffield, Sheffield, UK*

² *Department of Civil and Environmental Engineering, Imperial College London, London, UK*

* Corresponding author, E-mail: smmojtabaei1@sheffield.ac.uk

Abstract

Cold-formed steel (CFS) elements are increasingly used as main structural members in modern construction practice. While flexibility of CFS cross-sectional shape allows achieving higher load carrying capacities by using more efficient shapes, obtaining optimum design solutions can be a challenging task due to end-use constraints and complex behaviour of CFS elements controlled by local, global and distortional buckling modes. This study aims to develop a practical methodology for optimum design of CFS beam sections with maximum flexural strength and minimum deflection under ultimate and serviceability load conditions, respectively, in accordance with Eurocode 3 by taking into account manufacturing and end-use design constraints. Population-based Big Bang (BB) Crunch Optimisation method is employed to obtain optimum design solutions for twelve different CFS cross-sectional prototypes. To verify the flexural strength and stiffness of the optimum beam sections, detailed nonlinear finite element (FE) models are developed using ABAQUS by considering both material nonlinearity and initial geometrical imperfections. It is shown that the optimised sections based on serviceability limit state (SLS) and ultimate limit state (ULS) can provide, respectively, up to 44% higher effective stiffness and 58% higher bending moment capacity compared to a standard lipped channel beam section with the same plate width and thickness. Using plain channel and folded-flange sections generally leads to the best design solutions for SLS and ULS conditions, respectively. Finally, the results of detailed FE models are used to evaluate the adequacy of EC3 proposed procedures to estimate CFS beam capacity and deflection at ULS and SLS, respectively.

Key words

Cold-Formed Steel (CFS); Optimisation; Effective Width Method; Serviceability Limit State (SLS); Ultimate Limit State (ULS); Finite Element (FE) Analysis

1 Introduction

Cold-formed steel (CFS) load-bearing members and structural systems are increasingly used in modern construction, for example in modular buildings, stud wall systems, purlins, trusses, side rails and cladding. Although CFS elements are susceptible to local/distortional buckling, they can be more economical and efficient compared to similar hot-rolled sections, due to their inherent advantages such as high strength-to weight ratio, speed and efficiency of construction, and especially higher flexibility in manufacturing various profiles and sizes through cold-rolling or press-braking process at ambient temperature. The flexibility in CFS cross-sectional shapes provides an excellent opportunity to achieve higher load carrying capacities by using more efficient design solutions. However, this can be a challenging task due to typical manufacturing and end-use design constraints and complex behaviour of CFS elements controlled by combinations of local, global and distortional buckling modes. In general, optimisation of CFS members may aim to obtain an optimal cross-sectional shape without considering any restriction on the general shape of the sections (i.e. self-shape optimisation) (e.g. [1-7]), or determine optimum relative dimensions of a predefined cross-section (i.e. size optimisation) (e.g. [8-23]).

Different optimisation methods have been used for self-shape optimisation of thin-walled steel sections including Genetic Algorithm (GA) [1, 3, 4], Direct Multi-Search (DMS) method [2], graph theory and ant colony based algorithms [5], and gradient-based steepest descent method and simulated annealing [6]. In most of these studies, a steel sheet with a predefined total width is allowed to be bent at a certain number of locations, while the Direct Strength Method (DSM) [24] is generally adopted to estimate the compressive and bending capacity of the members. While considerable enhancement of strength were reported in all aforementioned self-shape optimisation methods, they may lead to impractical complex shapes with high manufacturing costs and/or difficulty in connecting to other structural components.

Several investigations have previously been conducted to optimise predefined standard CFS profiles such as C channels, and I and Z shape beams (e.g. [15, 16, 18]). It is shown that optimising the cross-sectional geometry of simply-supported CFS beams subjected to uniformly distributed vertical [10, 12, 13] or transverse load [14] can substantially improve their flexural capacity. However, due to cross-sectional

shape restrictions in size optimisation methods, the efficiency of the optimised sections may drop slightly from self-shape optimisation solutions [8, 9].

Ye et al. [25] extended the effective width method in EC3 [26] design of new type of folded-flange cross-section by considering the possible occurrence of multiple distortional buckling modes. Subsequently they used Particle Swarm Optimisation (PSO) method to increase the maximum flexural capacity of different cross-sectional prototypes and demonstrate the efficiency of the proposed folded flange sections. It was shown that, for the same amount of material, optimised folded-flange sections can provide up to 57% higher bending capacity compared to their standard counterparts. In another study, Ye et al. [10] adopted the Particle Swarm Optimisation (PSO) method to develop CFS beam sections with maximum flexural capacity, while Eurocode 3 (EC3) [26] design regulations and a number of manufacturing limitations were considered as design constraints. By using an extended EC3 effective width method, to take into account the possibility of multiple distortional buckling modes, they developed an optimum innovative folded-flange cross-section which could provide up to 57% higher flexural capacity compared to a standard benchmark section with the same plate width and thickness. In a follow-up study, Ye et al. [17] proposed an advanced shape optimisation framework to achieve maximum energy dissipation of CFS sections in uniaxial bending by providing a link between detailed nonlinear finite element analyses and PSO algorithm.

Various size optimisation methods have been also used to increase the compressive capacity of CFS axial members, such as Genetic Algorithm (GA) [18, 19], Particle Swarm Optimisation (PSO) [22] and Hough Transform [20]. Lee et al. [19] and Tian and Lu [21] optimised the geometry of CFS columns under compressive axial loads and proposed optimum design curves for different prescribed load levels. The local-flexural buckling strength of single CFS channels and global buckling strength of the CFS storage pallet racking cross-sections, determined according to the relevant EC3 (EN1993-1-3), have been also optimised by Ye et al [22] and Pastor et al. [23], respectively. In both studies, the adequacy of the optimum cross-sections was examined by the results of detailed FE analysis and experimental tests.

There is a general consensus that a structure must be designed to resist both service and extreme load conditions with the acceptable level of reliability during its effective life. However, the aforementioned literatures mainly focused on Ultimate Limit State (ULS), which conventionally represents the ultimate strength of the CFS structures under extreme load events. It should be noted that the level of slenderness for CFS elements is normally higher than hot-rolled steel counterparts, and therefore, the Serviceability Limit State (SLS) is generally more critical for CFS structures. For example, previous studies indicated that the serviceability criteria can govern the design of CFS frame systems

especially in low-seismic regions, e.g. under wind loads [27]. Violation of serviceability requirements (e.g. deflection limits) implies that the structure would be unfit for normal service operations.

To address to above mentioned research gaps, this study aims to provide a new framework for size optimisation of CFS beam members under both serviceability and ultimate limit states by considering manufacturing and design constraints. To obtain optimum cross-sections designed according to Eurocode design guidelines [26, 28, 29], a computationally efficient Big Bang (BB) Crunch (BB-BC) algorithm is adopted. The relative dimensions of the cross-sections, inclination of the flanges and lips, and adding features like different edge and intermediate stiffeners are considered as the main design variables in the proposed optimisation process. The efficiency of the optimum cross-sections is then compared with a standard conventional lipped-... nnel (1) all (1) benchmark (1) section. Subsequently, detailed GMNIA Finite Element (FE) models accounting for both material nonlinearity and initial geometrical imperfections are employed using ABAQUS [30] to evaluate the adequacy of EC3 methodology to estimate CFS beam capacity and deflection at ULS and SLS, respectively.

2 Eurocode Design Principals

Eurocode 3 (EC3) part 1-3 [26] specifies design requirements for CFS products made from thin gauge coated or uncounted steel sheet or strip. The EC3 design requirements are mainly based on limit state design, in which the structural performance is evaluated against various limiting conditions (e.g. ULS and SLS). In this paper, the flexural strength and stiffness of CFS beam elements are quantified according to the Effective Width Method adopted from EC3 part 1-3 [26] and EC3 part 1-5 [28]. The following subsections describe briefly the EC3 design procedure.

2.1 Local buckling

The EC3 effective width method can take into consideration the non-linear effect of local buckling, which leads to loss of strength in the middle of an internal plate element supported along both longitudinal edges, or in the free edge of an outstand element supported along one longitudinal edge. Therefore, the main load-bearing areas of the cross-section in compression zone are considered to be in the corner zones. Subsequently, the centroidal axis shifts towards the tensile part of the gross cross-section. The effective width of each internal and outstand compression element is calculated through the following equation in EC3 part 1-5:

$$\rho = \frac{b_e}{b} = \begin{cases} \frac{1}{\lambda_1} \left(1 - \frac{0.055(3 + \psi)}{\lambda_1} \right) & \text{for internal compression element} \\ \frac{1}{\lambda_1} \left(1 - \frac{0.188}{\lambda_1} \right) & \text{for outstand compression element} \end{cases} \quad (1)$$

where ρ is the plate width reduction factor, and b_e and b are the effective width and the total width of the plate, respectively. The effect of applied stress gradient is expressed by ψ , which is defined as the ratio of the plate end stresses. λ_1 is the slenderness ratio against local buckling and relates the material yield stress f_y to the elastic local buckling stress of the plate σ_{cr} :

$$\lambda_1 = \sqrt{\frac{f_y}{\sigma_{cr}}} \quad (2)$$

Estimation of the effective cross-section subjected to bending moment in EC3 generally requires an iterative process. This is referred to the fact that the stress gradient is changed due to shift of neutral axis of the effective cross-section, which depends on the loss of effective section in compression zone. While the iterative process is considered optional by EC3, in this study full iterations were carried out to achieve convergence.

2.2 Distortional buckling

Distortional buckling describes the distortion of the cross-section with rotation and translation at interior elements, leading to both in-plane and out-of-plane displacements of constituent plates. EC3 takes into account the local buckling and distortional buckling of CFS sections by reducing the effective width and the effective thickness of the constituent plates, respectively. The distortional slenderness, λ_d , can be calculated based on a simplified model, in which the restraining effects of the adjacent plates in the cross section are taken into account by using equivalent elastic springs:

$$\lambda_d = \sqrt{f_y / \sigma_{cr,s}} \quad (3)$$

where $\sigma_{cr,s}$ is the elastic buckling stress of the plate-stiffener assembly given by:

$$\sigma_{cr,s} = \frac{2\sqrt{KEI_s}}{A_s} \quad (4)$$

In the above equation, K and A_s are the stiffness of the spring (per unit length) and the effective cross-sectional area of the stiffener, respectively. E is the Young's modulus and I_s is the moment of inertia of the stiffener about the centroid parallel to the plate element. K is a function of the flexural stiffness of the adjacent plates and can be calculated based on the deflection of the stiffener assembly under a unit load $u = 1$ (per unit length). EC3 also recommends to use an iterative process to update the local slenderness ratio of the plates, λ_1 , by replacing $\lambda_{1,red} = \lambda_1 \sqrt{\chi_d}$. χ_d is the reduction factor corresponding to the distortional buckling resistance and can be calculated by using the relative slenderness λ_d . It should be mentioned that f_y should be substituted by $\sigma_{com} = \chi_d \cdot f_y$ in each iteration for the calculation of λ_d . This optional iteration loop was considered in this study until $\chi_{d,n} \approx \chi_{d,(n-1)}$. In this study, optional iteration loop was considered when the ratio of two consecutive loops ($\frac{\chi_{d,n}}{\chi_{d,(n-1)}}$) is between 0.99 and 1.01.

2.3 Global buckling

Based on EC3 part 1-1 [29], the design global buckling resistance moment of CFS beam members is taken as:

$$M_{b,Rd} = \frac{\chi_{LT} W_{eff} f_y}{\gamma_{M1}} \quad (5)$$

where W_{eff} is the effective modulus of the cross section and γ_{M1} is the partial safety factor prescribed by EC3, which is equal to 1.0. Also, χ_{LT} is the reduction factor corresponding to the lateral-torsional buckling (or global slenderness ratio), which is calculated based on the elastic critical moment of the beam member using the following equation:

$$\chi_{LT} = \sqrt{\frac{W_{eff} f_y}{M_{cr}}} \quad (6)$$

In common practice the CFS beams are generally laterally restrained by a floor system, which means the global instability (e.g. lateral-torsional buckling) of the CFS beam elements are practically prevented. Therefore, the global buckling modes are not considered in the optimum design of CFS beams in this study.

3 Problem Definition

The aim of the optimisation process in this study is to maximise the flexural capacity and stiffness of CFS beams under ULS and SLS conditions, respectively, calculated based on EC3. A standard lipped channel section that satisfies all EC3 design constraints (see Fig. 1) was selected as the starting point of the optimisation process. This section was also used as a benchmark to confirm the efficiency of the optimum design solutions. The total coil width of the steel plate $L = 453\text{mm}$ and its thickness $t = 1.8\text{mm}$ were kept constant during the proposed optimisation procedure to use the same amount of material in all cross sections. The radius of the rounded corners for all cross sections was assumed to be 3 mm. The elastic modulus, yield stress f_y and f_u of the steel material were taken as 210 GPa, $f_y = 450\text{MPa}$, and 0.3, respectively.

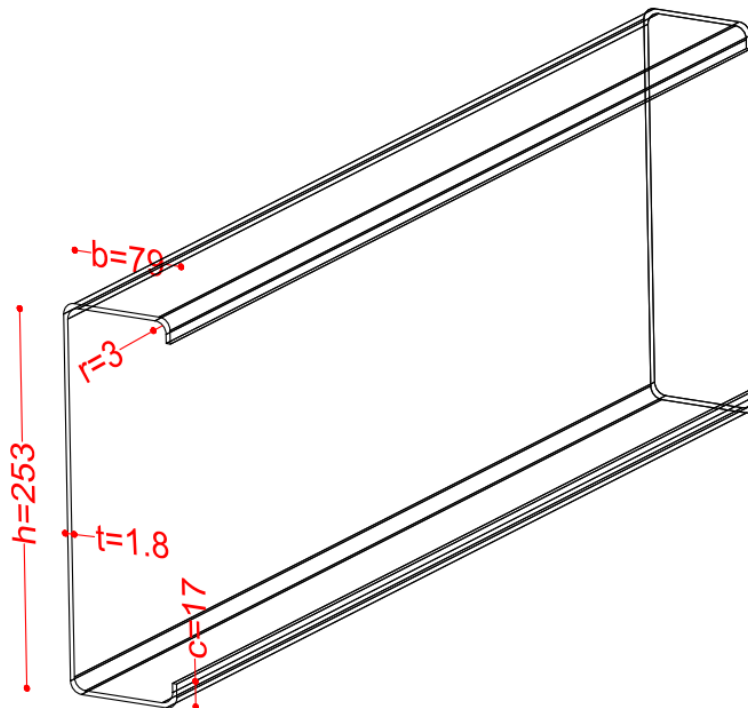


Fig. 1. Standard lipped channel section used as a benchmark dimension (mm)

In this study, 12 different prototypes were selected including conventional plain and lipped channels as well as those with single and double intermediate stiffeners (in web or flanges), single and double inclined edge stiffeners, and a newly developed folded flange channel. All selected shapes can be manufactured through cold-rolling or press-braking process (see Table 1) and can be potentially used in practical applications. Each prototype was individually optimised using different optimisation targets

(ULS and SLS). The following EC3 design constraints and practical and manufacturing limitations were imposed to each type of cross-sections as listed in Table 1:

a) The minimum width of the flange (bearing width) was set to be 50mm as suggested by SCI Guide ED-017 guidance [31]. This criterion was imposed to provide enough space for the connection of gypsum or wood based boards and decking to the CFS beams by using screws.

b) Based on the advice from the industrial collaborators of this project, the size of single and double lips was taken to be $c \geq 10$ mm, and $d \geq 5$ mm (see Table 1) to make the forming of edge stiffeners (lips) feasible by using conventional rolling or press-brake machines.

c) The minimum depth of the channel sections was assumed to be 200 mm, which allows a bolted connection or bridging to be constructed. By considering the standard floor depth, the maximum height of the web (beam depth) was also limited to 400 mm.

d) R_1 and R_2 factors were determined so that the web and flange intermediate stiffeners would be placed within the web height and flange width, respectively.

e) The EC3 limitations on the slenderness ratios (width to thickness), relative dimensions of the channels and angle of edge stiffeners were considered as design constraints as listed in Table 1.

f) The opening angle and the leg length of the intermediate stiffeners used in the web and flanges were set to be $\pi / 6$ and 15 mm, respectively, as recommended by the industrial partner of this project.

Table 1. Selected CFS beam prototypes, design variables and optimisation constraints

Prototypes	①	②	③	④	⑤	⑥
Cross-section						
Design variables	$x = b/L$	x_1, x_2, x_3	x_1, x_2, x_3	x_1, x_2, x_3, x_4, x_5	x_1, x_2, x_3, x_4, x_5	x_1, x_2, x_3, x_4, x_5
EC design constraints	$b, h/t$	$b, h/t$	$b, h/t$	$b, c, h, \pi/(2c)/4\pi$	$b, c, h, \pi/(2c)/4\pi$	$b, c, h, \pi/(2c)/4\pi$
Practical manufacturing limitations	$b \geq 50$	$b \geq 50, c \geq 10, d \geq 5$	$b \geq 50, c \geq 10, d \geq 5$	$b \geq 50, c \geq 10, d \geq 5$	$b \geq 50, c \geq 10, d \geq 5$	$b \geq 50, c \geq 10, d \geq 5$

Prototypes	7	8	9	10	11	12
C . ss-section						
Design variables	x_1 (b) x_2 (h) x_3 (θ_1) x_4 (θ_2)	x_1 (b) x_2 (h) x_3 (θ_1) x_4 (θ_2) x_5 (R_1) x_6 (R_2)	x_1 (b) x_2 (h) x_3 (θ_1) x_4 (θ_2) x_5 (R_1) x_6 (R_2)	x_1 (b) x_2 (h) x_3 (θ_1) x_4 (θ_2) x_5 (R_1) x_6 (R_2) x_7 (θ_1)	x_1 (b) x_2 (h) x_3 (θ_1) x_4 (θ_2) x_5 (R_1) x_6 (R_2) x_7 (θ_1) x_8 (θ_2)	x_1 (b) x_2 (h) x_3 (θ_1) x_4 (θ_2) x_5 (c)
EC design constraints	b (1) c (1) d (1) h (1) $\pi/3 \leq \theta_1 \leq 3/4\pi$	b (1) c (1) d (1) h (1) $\pi/3 \leq \theta_1 \leq 3/4\pi$	b (1) c (1) d (1) h (1) $\pi/3 \leq \theta_1 \leq 3/4\pi$	b (1) c (1) h (1) $\pi/3 \leq \theta_1 \leq 3/4\pi$	b (1) c (1) d (1) h (1) $\pi/3 \leq \theta_1 \leq 3/4\pi$	$7/12\pi \leq \theta_1 \leq 5/6\pi$ $\pi/3 \leq \theta_2 \leq 3/4\pi$
Practical manufacturing limitations	$b \geq 1$ $c \geq 1$ $d \geq 1$	$b \geq 1$ $c \geq 1$ $d \geq 1$	$b \geq 1$ $c \geq 1$ $d \geq 1$	$b \geq 1$ $c \geq 1$	$b \geq 1$ $c \geq 1$ $d \geq 1$	$b \geq 2b \sin(\theta_1)$

It should be noted that the design constraints listed in Table 1, especially in terms of channel dimensions, are typically related to the other elements connected to the CFS beam such as trapezoidal decking, plywood boards and angle cleats.

4 Big Bang-Big Crunch algorithm

Big bang-big crunch (BB-BC) optimisation method was first proposed by Erol and Eksin [32] based on the big bang and big crunch theories of the universe evolution. In this method, the randomness of the candidates and their convergence to the optimum solution represent the energy dissipation and gravitational attraction in nature. Previous studies demonstrated that, in general, the BB-BC optimisation method can offer several advantages such as lower computational time, higher convergence speed, and simpler programming compared to other conventional heuristic algorithms such as Genetic Algorithm (GA), Particle Swarm Optimisation (PSO) and Ant Colony Optimisation [33-35]. This is especially important for the complex optimisation of CFS elements due to their nonlinear behaviour affected by local and distortional buckling modes.

In the BB-BC optimisation process, the candidate solutions are randomly distributed over the search space (Big Bang phase) and then a convergence operation is used to calculate a weighted average of the candidate solutions (Big Crunch phase). In the big bang phase, the candidate solutions are uniformly distributed over the search space. The convergence operator in Big Crunch phase is then used to calculate the fitness function of each candidate and update its current position. The convergence operator is defined as the weighted average of the position of candidate solutions with respect to the inverse of the penalized fitness function, and is calculated as:

$$X_{cm} = \frac{\sum_{i=1}^{nc} \frac{1}{f_i} X_i}{\sum_{i=1}^{nc} \frac{1}{f_i}} \quad (7)$$

where X_{cm} and X_i are the position of the centre of mass and i^{th} candidate in the n -dimensional search space, f_i is the penalized fitness function for i^{th} candidate, and nc is the candidate population size.

The positions of the candidate solutions for the next iteration of the Big Bang are normally distributed around the centre of mass, X_{cm} , using the following equation:

$$X_i^{new} = X_{cm} + \sigma \quad (8)$$

where X_i^{new} is the position of the new candidate solution i , and σ is the standard deviation corresponding to a subset of the search space. In the proposed method, σ decreases inversely with each succeeding Big Bang iteration using the following equation:

$$\sigma = \frac{r\alpha(X_{max} - X_{min})}{s} \quad (9)$$

where r is a random number from a standard normal distribution, α is a parameter used to limit the size of the search space, X_{min} and X_{max} represent the lower and upper limits of the selected design variables, and s is the number of Big Bang iterations. In this study, the number of candidate population size (nc) and number of Big Bang iterations (s) were taken, respectively, as 150 and 100 for the first 6 prototypes of cross-sections, and 200 and 150 for the other prototypes. Parameter α was also selected equal to 1.0. Fig. 2 shows the details of the flowchart for the BB-BC algorithm used in this study.

It should be noted that, for the optimisation problems in this study, the only design constraints are EC3 and manufacturing restrictions imposed on the input design variables (see Table 1). Therefore, the constraints can be easily handled by using a domain (max and min values) for each design variable.

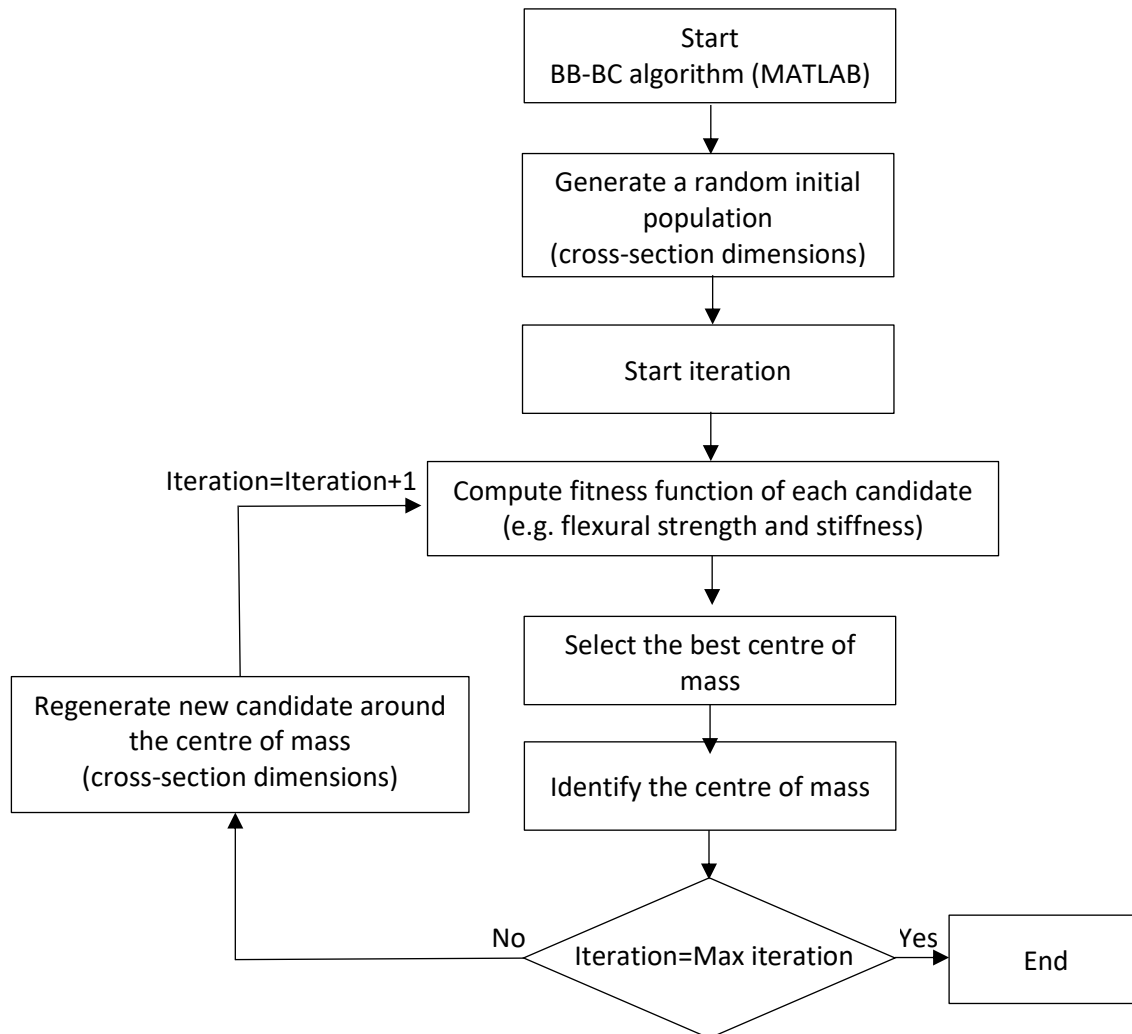


Fig. 2. Big Bang–Big Crunch algorithm flowchart.

5 Optimum Design of CFS Beams

The optimisation framework was conducted on the selected prototypes (see Table 1) by developing two programmes MATLAB [36] to design CFS beams based on EC3 design regulations and to carry out BB-BC. The optimisation process was aimed at obtaining the optimum relative dimensions of each cross-section as well as the best positions of the edge and intermediate stiffeners in web and flanges.

To ensure that the optimum results are consistent, each prototype was optimised three times using randomly selected candidates. While the maximum difference between the results obtained from the three runs was always less than 1%, the best design solution was selected. During the optimisation process, the convergence was normally achieved after approximately 20 and 50 steps for the ① to ⑩ and ⑦ to ⑫ prototypes, respectively. As an example, the iteration history of the optimisation process for the prototype $\bar{A}①$ is shown in Fig. 3, where the convergence is achieved after 18 iterations for all three cases.

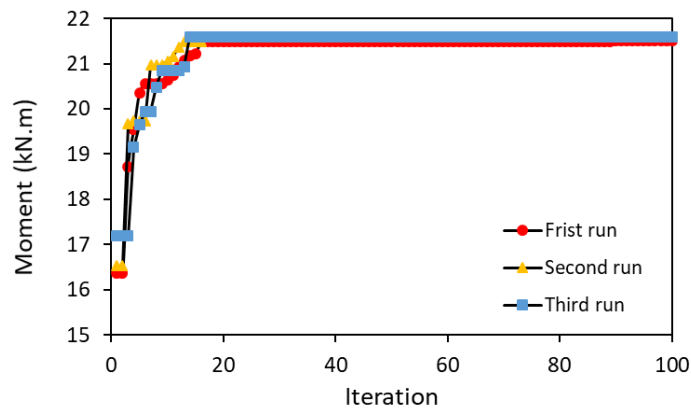


Fig. 3. Iteration history of the optimisation algorithm (BB-BC) for prototype $\bar{A}①$.

5.1 Optimisation for Ultimate Limit State (ULS)

This section is aimed to optimise laterally braced CFS beams in order to maximize their bending capacity at ULS. In this case, the optimisation target can be represented as a function of the effective property of the cross-section defined by:

$$\text{Max } M(x) = W_{\text{eff}} f_y / \gamma_{M_0} \quad X_i^L \leq X_i \leq X_i^U, \quad (i = 1, \dots, n) \quad (10)$$

where $M(x)$ and W_{eff} are the design moment resistance and effective section modulus of a cross-section about the major axis, respectively. W_{eff} is the ratio of effective second moment of inertia I_{eff} to the distance from effective centroid to furthest compression fibre, calculated by considering the contribution of all effective parts of the cross section. γ_{M_0} is a partial safety factor used for ultimate limit state and is considered to be 1.0 as prescribed by EC3 [29]. The lower and upper bound of each design variable (X_i^L and X_i^U) are obtained based on the EC3 design requirements and the practical and manufacturing limitations listed in Table 1.

Table 2 compares the flexural capacity and dimensions of the standard section and those optimised based on maximum bending moment capacity for all selected prototypes using the same amount of material. The standard lipped channel section has been used as a benchmark to assess the efficiency of the proposed optimisation methodology. It is shown that the proposed optimisation method could considerably (up to 58%) increase the maximum bending capacity of the standard section. For better comparison, the effective cross-section of the optimum solutions are presented in Table 3, in which the effective parts of cross-sections are drawn by thick solid black lines. The thickness of the effective parts are reduced in the location of the intermediate and edge stiffeners to take into account distortional buckling modes as discussed in Section 2.2.

Based on the ULS optimisation results in Table 2, the following conclusions can be drawn:

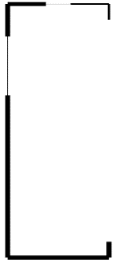



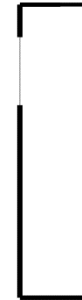


- The flexural capacity of the benchmark lipped channel is increased by 30% only by optimising its relative cross-sectional dimensions (prototype .). An additional 10% higher flexural capacity can be obtained by using an optimised CFS channel with double edge stiffener (prototype ⑦). It should be noted that the efficiency of the proposed optimisation method would be considerably increased by using more flexible design constrains (i.e. a wider range of input design variables).
- In general, plain channel sections (prototypes ①, ② and ③) do not provide efficient design solutions even after optimisation. This is referred to the fact that plain channels are generally highly susceptible to the local buckling of flanges.
- The flexural capacity of the optimum single and double lipped channels (prototypes \bar{A} ① and ⑦) are not generally enhanced by incorporating intermediate stiffeners in the web (prototypes ⑤, ⑥, \bar{A} ①① and ⑱). This is especially evident in the case of double intermediate web stiffeners (prototypes ⑥ and ⑨). This shows the inefficiency of using web stiffeners in the tension zone of the cross-section. Besides, folding the intermediate stiffeners into the section results in a reduction of the web height (noting that total coil width is kept constant), which in turn reduces the flexural capacity of the section.
- Comparison between prototypes \bar{A} ① and ⑩, and prototypes ⑨ and ⑪ indicates that adding intermediate flange stiffeners can increase (up to 17%) the moment capacity of the sections. The optimum location of the flange intermediate stiffener is approximately in the middle of the flange.
- As a general trend, it can be seen that optimised cross-sections tend to adopt taller web and subsequently narrower flanges. Therefore, all prototypes were optimised towards minimum specified flanges of 50 mm. As shown in Table 2, using folded flange section (prototype ⑫) provides the highest flexural capacity among all selected prototypes and offers 58% more flexural strength

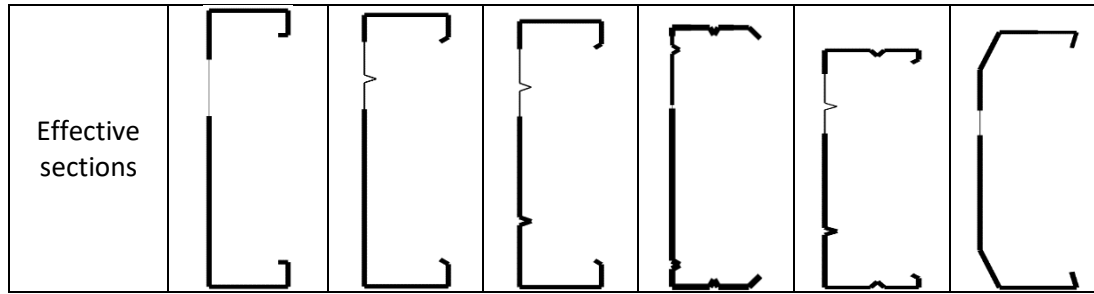
compared to the benchmark section. The folded flange cross-section can be easily manufactured (only 6 bends are needed) compared to the channels with intermediate stiffeners, and therefore, can provide a practical and efficient design solution.

Table 2. Dimensions and flexural capacity of standard and optimum CFS beams for different prototypes at ULS

Prototype	h (mm)	b (mm)	c (mm)	d (mm)	θ_1°	θ_2°	R_1	R_2	M_{\max} (kN m)	$\frac{M_{\max}}{M_{\max, \text{standard}}}$
Standard	261	79	17						16.47	1
①	353	50							15.56	0.94
②	338	50					0.842		17.16	1.04
.	323	50					0.195		15.81	0.96
④	305	50	24		89				21.40	1.30
⑤	290	50	24		91		0.774		21.22	1.29
⑥	274	50	25		92		0.215		19.68	1.19
⑦	285	50	27	7	90				23.63	1.43
⑧	276	50	24	7	135		0.760		22.03	1.34
⑨	263	50	24	6	135		0.250		20.41	1.24
⑩	262	50	15		135		0.100	0.545	23.75	1.44
⑪	258	50	12	6	135		0.256	0.555	21.86	1.33
⑫	217	48	50	20	100	79			25.97	1.58

Table 3. The effective cross-section of optimum CFS beams for different prototypes at ULS

Prototypes	Benchmark	①	②	③	④	⑤	⑥
Effective sections							
Prototypes	⑦	⑧	⑨	⑩	⑪	⑫	



5.2 Optimisation for Serviceability Limit State (SLS)

The serviceability limit state (SLS) is generally defined as the condition beyond which a structure becomes unfit for service. Unlike ULS, SLS depends more on the stiffness rather than the strength of a structural system. Based on Eurocode [37], the structural reliability under either SLS or ULS can be represented by the following inequality:

$$R_d \geq R_{Ed} \quad (11)$$

where R_d is the design resistance and R_{Ed} is the design load effect calculated for persistent and transient design situations as follow:

$$R_{Ed} = \sum_{j \geq 1} \gamma_{G,j} \cdot G_{k,j} + \gamma_{Q,1} \cdot Q_{k,1} \quad (12)$$

In Eq. 12, $\gamma_{G,j}$ and $G_{k,j}$ are the partial safety factor and characteristic value for permanent action j , while $\gamma_{Q,1}$ and $Q_{k,1}$ are the partial safety factor and characteristic value of the leading variable action 1, respectively. Eurocode [37] distinguishes between SLS and ULS by means of partial safety factors, which are $\gamma_{G,j} = 1.35$ and $\gamma_{Q,1} = 1.5$ for ULS and $\gamma_{G,j} = \gamma_{Q,1} = 1$ for SLS. While in general serviceability limit state loading condition should be determined for each specific project, the ratio of service to ultimate loads (or the ratio of average partial safety factors for SLS over those for ULS) in this study was taken as 0.7 and kept constant for different prototypes during the optimisation process. Therefore, to design for serviceability based on EC3 [28], the maximum compressive stress $\sigma_{com,Ed.ser}$ in each cross-section was calculated based on the effective cross-section under $M_{Ed,ser} = 0.7 M_{max}$ as shown in Fig. 4:

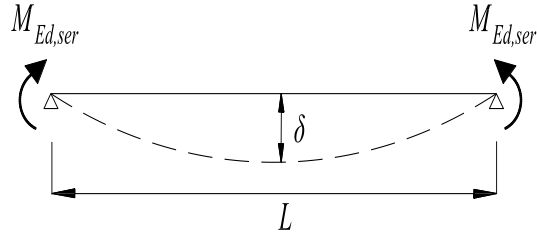


Fig. 4. Beam deflection at SLS subjected to a uniform pure bending ($M_{Ed,ser}$)

To determine the effective second moment of area (I_{eff}) of the CFS beam section, the slenderness ratio is calculated from:

$$\bar{\lambda}_{p,ser} = \bar{\lambda}_p \sqrt{\frac{\sigma_{com,Ed,ser}}{f_y}} \quad (13)$$

For serviceability design, the optimisation problem can be formulated as a minimisation of beam deflection subjected to pure bending moment, which is defined by:

$$\text{Min } f(x) = \frac{M_{Ed,ser} L^2}{8EI_{fic}} \quad X_i^L \leq X_i \leq X_i^U, \quad (i=1, \dots, n) \quad (14)$$

where $f(x)$ is the deflection of the CFS beam. X_i is the design variables with the lower and upper bounds of X_i^L and X_i^U , specified in Table 1, respectively. In order to provide reasonable comparison between the behaviour of each prototype at its SLS, the length of the beam is kept constant and equal to $L = 5000\text{mm}$. I_{fic} is the effective second moment of area, which is based on the service load. Eurocode 3 part 1-3 [26] stipulates that the properties of the effective cross section explained in Section 2 must be used in all SLS checks for CFS members. Also, it has been mentioned that the second moment of area of CFS sections can be estimated by an interpolation between effective and gross cross sections for the design load combination using the following expression:

$$I_{fic} = I_{gr} - \frac{\sigma_{gr}}{\sigma} (I_{gr} - I(\sigma)_{eff}) \quad (15)$$

where I_{gr} is the second moment of area of the gross cross section, σ_{gr} is the maximum compressive bending stress based on the gross cross section at serviceability limit state (SLS), and $I(\sigma)_{eff}$ is the second moment of area of the effective cross section by considering local buckling estimated based on

maximum stress $\sigma \geq \sigma_{gr}$ (σ is the highest absolute value of stress within the beam length).

Subsequently, σ and σ_{gr} can be calculated based on the following equations:

$$\sigma_{gr} = \frac{M_{Ed,ser}}{W_{ser}} = \frac{M_{Ed,ser}}{I_{gr} / z_{c,ser}} \quad (16)$$

$$\sigma = \frac{M_{max}}{W_{eff}} = f_y \quad (17)$$

In the above equations, W_{ser} and W_{eff} are the section modulus for the SLS and ULS, respectively, and $z_{c,ser}$ represents the distance of neutral axis to extreme compression fibre in a CFS section associated with SLS. By substituting Eq. 10 in Eq. 17, the maximum stress corresponding to local buckling, σ , would be equal to the yield stress f_y .

The cross-sectional dimensions, second moment of area and flexural capacity of optimum sections for each prototype under service load level are calculated as presented in Table 4. Based on the results, the following observations can be drawn:

- The dimensions of the optimum plain channels (prototypes ①, ② and .) for SLS are very similar to those optimised for ULS (the only difference is in the optimum locations of the web stiffeners). Unlike optimisation for ULS, optimum plain channels at SLS could provide considerably higher effective stiffness (up to 44%) compared to the benchmark lipped channel section. However, the flexural capacity of the sections may be slightly (up to 10%) lower than the benchmark channel. This implies that, in general, optimum plain channels are more efficient to satisfy SLS checks.
- The flexural stiffness of optimum plain and single/double lipped channels (prototypes ①, \bar{A} ① and ① \bar{A} ①) were reduced by incorporating intermediate web stiffeners. Similar to the ULS optimisation, this reduction is more evident in the case of double intermediate web stiffeners (prototypes ③, ⑥ and ⑨). However, it can be seen from Table 4 that using optimised intermediate flange stiffeners (prototypes ⑩ and ⑪) could increase the effective stiffness and capacity of the sections by up to 10% and 27%, respectively.
- By optimising the relative dimensions of the standard benchmark section at SLS, the flexural stiffness and capacity of the section can be increased by 37% and 11%, respectively. However, for the same amount of material, optimisation of the channel section with folded flanges (prototype ⑫) resulted in a noticeable increase (up to 52%) in both effective stiffness and capacity of the

standard section. This highlights the efficiency of folded flange sections for both ultimate and serviceability limit states.

- While a negligible difference (less than 4%) is seen between the effective stiffness of the optimum beams with single and double edge stiffeners (prototypes ① and ⑫), respectively) at SLS, the flexural capacity of the section with double edge stiffener is 13% higher than the one with single edge stiffener. A similar trend is observed for the sections with the intermediated web stiffeners (prototypes ⑤ and ⑥ compared to prototypes ⑧ and ⑨).

Table 4. Dimensions, effective second moment of area and flexural capacity of standard and optimum CFS beams for different prototypes at SLS

Prototype	$\frac{M_{ser}}{M_{max}}$	h (mm)	b (mm)	c (mm)	d (mm)	θ_1 (deg)	θ_2 (deg)	R ₁	R ₂	I_{fic} ($\times 10^6$) (mm ⁴)	$\frac{I_{fic}}{I_{fic,standard}}$	M _{max} (kN m)	$\frac{M_{max}}{M_{max,standard}}$
Standard	0.7	261	79	17						7.22	1	16.47	1
①	0.7	353	50							10.39	1.44	15.53	0.94
②	0.7	338	50					0.9		10.33	1.43	16.29	0.99
③	0.7	323	50					0.1		9.01	1.25	14.86	0.90
④	0.7	333	50	10		135				9.88	1.37	18.24	1.11
⑤	0.7	318	50	10		135		0.9		9.20	1.27	17.68	1.07
⑥	0.7	303	50	10		135		0.1		8.55	1.18	16.69	1.01
⑦	0.7	323	50	10	5	90				9.65	1.34	20.61	1.25
⑧	0.7	308	50	10	5	135		0.9		8.91	1.23	19.34	1.17
⑨	0.7	293	50	10	5	135		0.1		8.23	1.14	17.96	1.09
⑩	0.7	273	50	10		135		0.1	0.800	9.31	1.29	22.29	1.35
⑪	0.7	263	50	10	5	135		0.1	0.319	8.71	1.22	20.86	1.27
⑫	0.7	227	48	50	15	105	65			10.10	1.41	24.99	1.52

- Similar to the ULS optimisation, optimised cross-sections tend to use taller web and narrower flanges. Therefore, all optimised sections have the minimum specified flange width of 50 mm. The main differences between optimised shapes for ULS and SLS are the size and angle of the edge stiffeners and the location of the intermediate web and flange stiffeners.

- Optimisation of the CFS beam sections at SLS on average increased the flexural stiffness and strength of the standard benchmark section by 30% and 14%, respectively. However, comparisons between the results presented in Tables 2 and 4 indicates that the sections optimised at SLS exhibit on average 9% lower flexural strength compared to those optimised at ULS.

6 Analytical Investigation

The ultimate flexural capacity and deflection of the standard and optimised cross-sections listed in Table 1 were determined at ULS and SLS using detailed nonlinear FE models in ABAQUS [30], where the effects of material nonlinearity and initial geometric imperfections were taken into account. The results were then used to evaluate the efficiency of the proposed optimisation method in obtaining sections with reduced maximum deflection at SLS and increased ultimate capacity at ULS. The detailed FE models were also used to assess the accuracy of Eurocode predictions for different prototypes. It should be noted that the capability of detailed finite element (FE) models to simulate both pre- and post-buckling behaviour of CFS sections has been demonstrated in previous studies provided that appropriate element types, material models and geometric imperfections are adopted [22, 38-40]. The adopted FE models have been also validated against a series of experimental tests on CFS back-to-back channels conducted at The University of Sheffield by the authors [13].

6.1 Detailed FE models

The detailed FE models of the CFS sections corresponding to the selected prototypes were developed in ABAQUS [30] using a 4-noded quadrilateral shell element with reduced integration (S4R). Based on a comprehensive mesh sensitivity analyses, a mesh size of $10 \times 10 \text{ mm}$ was found to be appropriate since a further mesh refinement did not make any noticeable change in the results. The stress-strain behaviour of CFS plates was modelled by using the widely adopted constitutive model proposed by Haidarali and Nethercot [41]:

$$\varepsilon = \frac{\sigma}{E} + 0.002 \left(\frac{\sigma}{\sigma_{0.2}} \right)^n \quad \text{for } \sigma \leq \sigma_{0.2}$$

$$\varepsilon = \varepsilon_{0.2} + \frac{100(\sigma - \sigma_{0.2})}{E} \quad \text{for } \sigma \geq \sigma_{0.2}$$
(18)

where $\sigma_{0.2}$ and $\varepsilon_{0.2}$ are the 0.2% proof stress and the total strain at $\sigma_{0.2}$, respectively. n is a shape parameter recommended by Gardner and Ashraf [42] to be taken as 28 for grades 350 and 450 steel, and E is the elastic modulus which is taken equal to 210 GPa. The effects of geometrical imperfections

were taken into account in CFS sections by performing eigenvalue elastic buckling analysis which is available in ABAQUS library [30] on the CFS beams. The obtained dominant buckling mode (either local or distortional) was then incorporated in the initial perfect geometry of the cross-section and scaled to the certain magnitude extracted from the Cumulative Distribution Function (CDF) values suggested by “ ① .. d (Peköz [43]). In this study, a CDF value of 50% was adopted (corresponding to $0.34t$ and $0.94t$ for local and distortional imperfections, respectively). It should be mentioned that the adopted CDF values are valid for the sections with the thickness (t) less than 3mm [43], so they are suitable for the sections considered in this study.

As shown in Fig. 5, the pinned support at the two ends of the CFS beam about major axis was simulated by coupling the nodes at each end section to the reference point defined in the mid-web, while the rotation about the minor axis was prevented. The end sections were also prevented from warping to be consistent with the assumption made for the EC3 design calculations in Section 5. To avoid lateral-torsional buckling, lateral bracings (representative of transitive beams in the roof systems) were used at each L/4 along the length of beam (see Fig. 5).

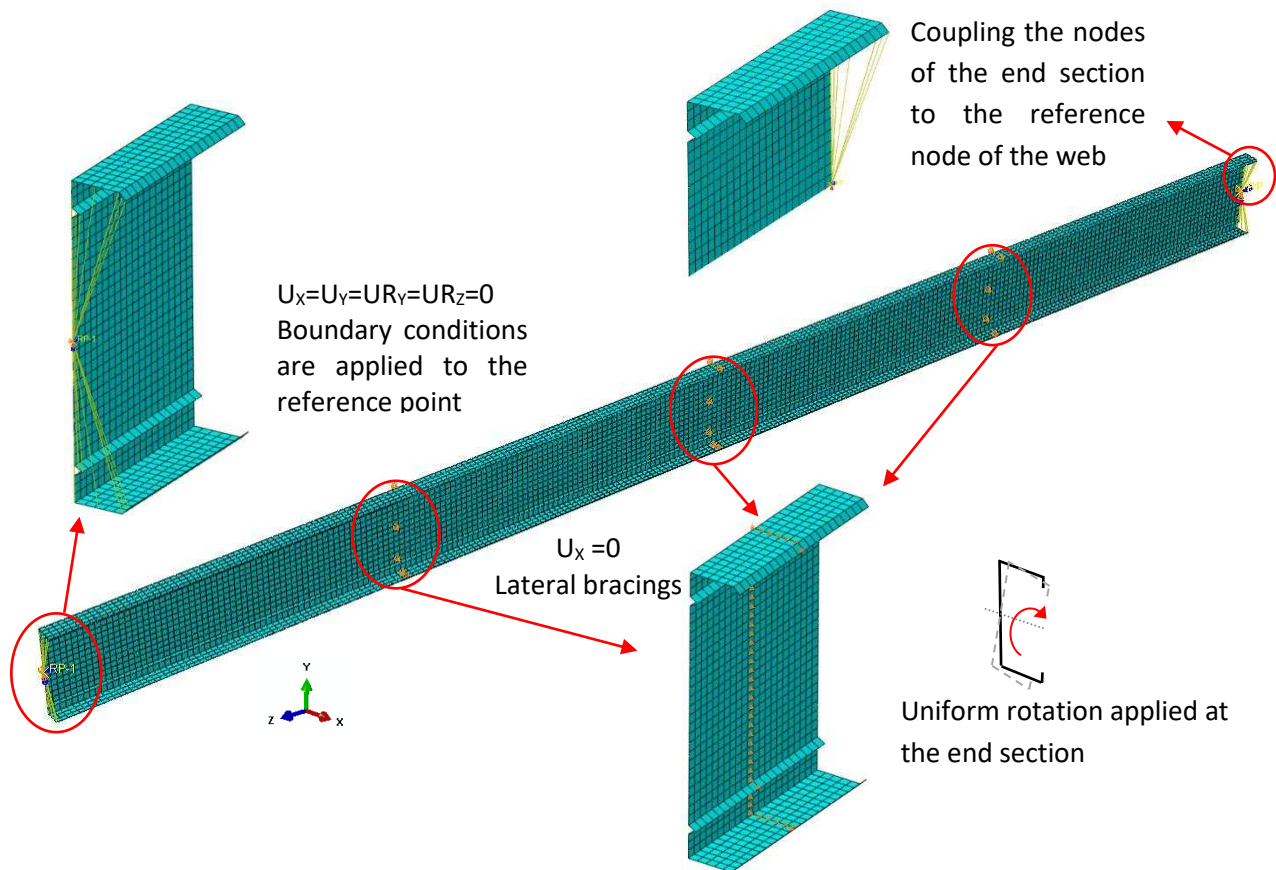


Fig. 5. Boundary conditions in the FE models subjected to pure bending moment

While the pure bending moments at SLS (equal to 70% of the calculated flexural capacity according to EC3) were directly imposed at the two end sections of the beam, the external loads at ULS were simulated by applying uniform rotations about the major axis of the two end sections using a displacement control regime. FE analysis was carried out using IAI General Method analysis available in ABAQUS library [30], which has been shown to be capable of accurately predicting the flexural capacity and deformation of CFS elements at both pre- and post- buckling range [10, 17, 44].

6.2 FE results of the standard and optimum sections

The results of the non-linear FE analyses were used to assess the efficiency of the CFS beam sections optimised using different prototypes (obtained in Section 5) compared to the benchmark section. Table 5 lists the maximum deflections and flexural capacities of the 12 selected prototypes as well as the benchmark channel predicted by EC and FE at SLS and ULS. Generally, the results obtained from EC are shown to be reliable for both SLS and ULS. The average ratios of the calculated mid-span deflection and flexural capacity using EC3 to the corresponding FE results were 1.01 and 1.02 with standard deviation of 8% and 5%, respectively. This implies that effective stiffness (I_{fic}) and effective second moment of area (I_{eff}) calculated based on EC3 effective width method provide reasonable predictions.

Fig. 6 compared the moment versus mid-span deflection curves for the CFS beam with standard and optimum cross-sections (under ULS) for prototype ① and ⑨ as representative examples. It is shown that the proposed optimisation algorithm could increase both stiffness and maximum capacity of the sections. Fig. 7 also illustrates the typical failure mode of the CFS beam at ULS, which is due to the local/distortional buckling at the compression zone.

Table 5. EC3 and FE results of CFS beam with benchmark and optimum cross-sections in terms of maximum deflection and flexural capacity at SLS and ULS, respectively.

Prototype	SLS			ULS		
	δ_{EC} (mm)	δ_{FE} (mm)	$\frac{\delta_{EC}}{\delta_{FE}}$	$M_{max,EC}$ (kN m)	$M_{max,FE}$ (kN m)	$\frac{M_{max,EC}}{M_{max,FE}}$
Benchmark	23.8	22.9	1.04	16.47	16.94	0.97
①	15.5	17.6	0.88	15.56	14.94	1.04
②	16.5	17.9	0.92	17.16	16.36	1.05
③	17.2	18.0	0.95	15.81	15.11	1.05
④	19.2	21.9	0.88	21.40	22.36	0.96
⑤	20.0	21.4	0.94	21.22	21.93	0.97

.	20.3	19.4	1.05	19.68	19.62	1.00
⑦	22.3	22.2	1.00	23.63	24.22	0.98
⑧	22.7	20.3	1.12	22.03	22.68	0.97
⑨	22.8	21.1	1.08	20.41	19.72	1.03
⑩	25.0	23.2	1.08	23.75	21.12	1.12
⑪	24.9	23.1	1.08	21.86	19.97	1.09
⑫	25.8	24.3	1.06	25.97	23.92	1.09
⑬ Average			1.01			1.02
⑭ Standard Deviation			0.082			0.055

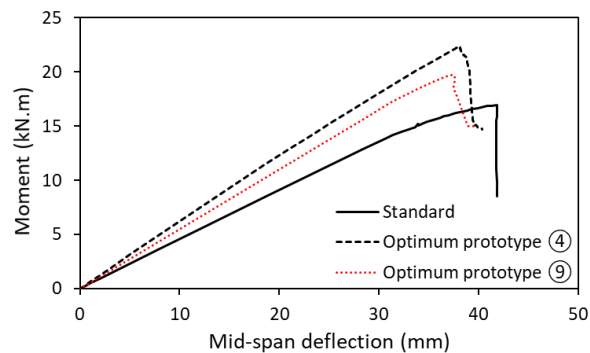


Fig. 6. Moment versus mid-span deflection curve for the CFS beam with standard and optimum cross-sections for prototypes ④ ①A ⑨

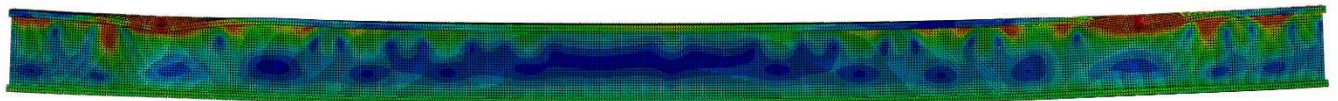


Fig. 7. Typical failure mode of the CFS beam at ULS

7 Summary and conclusions

A new optimisation framework was presented to develop more economical laterally braced CFS beam based on serviceability and ultimate limit states, according to EC3 effective width method, by optimising the relative dimensions of cross-sections and allowing for the inclined single or double edge lips and triangular intermediate web and flange stiffeners. To obtain optimum solutions, Big Bang Big Crunch (BB-BC) optimisation algorithm was adopted while design variables were determined by taking into account EC3 design constraints as well as a range of manufacturing and end-use limitations. The proposed optimisation framework was applied on twelve different prototypes and the accuracy of the

results at both SLS and ULS was examined through detailed FE models. Based on the results presented in this paper, the following conclusions could be drawn:

1. For the same amount of material, the proposed optimisation framework could increase the flexural capacity and stiffness of the standard benchmark section by 58% and 44%, respectively. In general, optimised cross-sections (at both SLS and ULS) tend to use taller web and narrower flanges. The main differences between optimised shapes for ULS and SLS are the size and the angle of edge stiffeners as well as the location of the intermediate web and flange stiffeners.
2. The optimum dimensions of the plain channels for SLS are very similar to those obtained for ULS. While optimisation of plain channel sections (including those with intermediate stiffeners) at ULS did not provide efficient design solutions, using optimum plain channels at SLS could offer considerably higher stiffness compared to the benchmark lipped channel section. This implies that optimum plain channels are more adequate for SLS requirements.
3. The flexural capacity and stiffness of the benchmark lipped channel at ULS and SLS was increased by 30% and 37%, respectively, only by optimising its relative cross-sectional dimensions. While an additional 10% flexural capacity at ULS was obtained by using double edge stiffeners, a negligible improvement in flexural stiffness was observed at SLS.
4. The flexural capacity and stiffness of the optimum single and double lipped channels at ULS and SLS, respectively, were not generally enhanced by incorporating intermediate stiffeners in the web. However, adding intermediate stiffeners in the flanges could increase the flexural capacity and stiffness of the sections at ULS and SLS by up to 17% and 10%, respectively.
5. It was shown that the newly developed folded flange channel can be considered as the most desirable section owing to the fact that it is capable to provide 58% and 41% higher bending capacity and stiffness at ULS and SLS, respectively, compared to the standard lipped channel section with the same amount of material.
6. The efficiency of the optimised CFS beam sections was assessed by using detailed FE models accounting for material non-linearity and initial geometric imperfections. The results of the FE simulations in general confirm the accuracy of the mid-span deflection and flexural capacity of the sections predicted by EC3 proposed methodology (less than 12% error).

Acknowledgment

This research was supported by the Engineering and Physical Sciences Research Council (EPSRC) grant EP/L019116/1. The first author was also supported by EPSRC Doctoral Scholarship grant 1625179. The authors would like to thank the EPSRC for their financial support and express their gratitude to BW Industries for their invaluable consultation.

Reference

- [1] B. Wang, G.L. Bosco, B.P. Gilbert, H. Guan, L.H. Teh, Unconstrained shape optimisation of singly-symmetric and open cold-formed steel beams and beam-columns, *Thin-Walled Structures*, 104 (2016) 54-61.
- [2] J.F.A. Madeira, J. Dias, N. Silvestre, Multiobjective optimization of cold-formed steel columns, *Thin-Walled Structures*, 96 (2015) 29-38.
- [3] B.P. Gilbert, T.J.M. Savoyat, L.H. Teh, Self-shape optimisation application: Optimisation of cold-formed steel columns, *Thin-Walled Structures*, 60 (2012) 173-184.
- [4] B.P. Gilbert, L.H. Teh, H. Guan, Self-shape optimisation principles: Optimisation of section capacity for thin-walled profiles, *Thin-Walled Structures*, 60 (2012) 194-204.
- [5] P. Sharafi, L.H. Teh, M.N.S. Hadi, Shape optimization of thin-walled steel sections using graph theory and ACO algorithm, *Journal of Constructional Steel Research*, 101 (2014) 331-341.
- [6] J. Leng, J.K. Guest, B.W. Schafer, Shape optimization of cold-formed steel columns, *Thin-Walled Structures*, 49 (2011) 1492-1503.
- [7] H. Liu, T. Igusa, B.W. Schafer, Knowledge-based global optimization of cold-formed steel columns, *Thin-Walled Structures*, 42 (2004) 785-801.
- [8] J. Leng, Z. Li, J.K. Guest, B.W. Schafer, Shape optimization of cold-formed steel columns with fabrication and geometric end-use constraints, *Thin-Walled Structures*, 85 (2014) 271-290.
- [9] B. Wang, B.P. Gilbert, H. Guan, L.H. Teh, Shape optimisation of manufacturable and usable cold-formed steel singly-symmetric and open columns, *Thin-Walled Structures*, 109 (2016) 271-284.
- [10] J. Ye, I. Hajirasouliha, J. Becque, A. Eslami, Optimum design of cold-formed steel beams using Particle Swarm Optimisation method, *Journal of Constructional Steel Research*, 122 (2016) 80-93.

- [11] J. Lee, S.M. Kim, H.S. Park, B.H. Woo, Optimum design of cold-formed steel channel beams using micro-genetic algorithm, *Eng. Struct.*, 27 (2005) 17–24.
- [12] K. Magnucki, M. Rodak, J. Lewiński, Optimization of mono- and anti-symmetrical I-sections of cold-formed thin-walled beams, *Thin-Walled Structures*, 44 (2006) 832-836.
- [13] J. Ye, S.M. Mojtabaei, I. Hajirasouliha, P. Shepherd, K. Pilakoutas, Strength and deflection behaviour of cold-formed steel back-to-back channels, *Engineering Structures*, 177 (2018) 641-654.
- [14] T. Tran, L.-y. Li, Global optimization of cold-formed steel channel sections, *Thin-Walled Structures*, 44 (2006) 399-406.
- [15] H. Adeli, A. Karim, Neural network model for optimization of cold-formed steel beams, *J. Struct. Eng. ASCE* 123, (1997) 1535–1543.
- [16] A. Karim, H. Adeli, Global optimum design of cold-formed steel hat-shape beams, *Thin-Walled Structures*, 35 (1999) 275-288.
- [17] J. Ye, J. Becque, I. Hajirasouliha, S.M. Mojtabaei, J.B.P. Lim, Development of optimum cold-formed steel sections for maximum energy dissipation in uniaxial bending, *Engineering Structures*, 161 (2018) 55-67.
- [18] W. Ma, J. Becque, I. Hajirasouliha, J. Ye, Cross-sectional optimization of cold-formed steel channels to Eurocode 3, *Engineering Structures*, 101 (2015) 641-651.
- [19] J. Lee, S.M. Kim, H.S. Park, B.H. Woo, Optimum design of cold-formed steel columns by using micro genetic algorithms, *Thin-Walled Structures*, 44 (2006) 952–960.
- [20] B. Wang, B.P. Gilbert, A.M. Molinier, H. Guan, L.H. Teh, Shape optimisation of cold-formed steel columns with manufacturing constraints using the Hough transform, *Thin-Walled Structures*, 106 (2016) 75-92.
- [21] Y.S. Tian, T.J. Lu, Minimum weight of cold-formed steel sections under compression, *Thin-Walled Structures*, 42 (2004) 515-532.
- [22] J. Ye, S.M. Mojtabaei, I. Hajirasouliha, Local-flexural interactive buckling of standard and optimised cold-formed steel columns, *Journal of Constructional Steel Research*, 144 (2018) 106-118.
- [23] M.M. Pastor, M. Casafont, E. Chillarón, A. Lusa, F. Roure, M.R. Somalo, Optimization of cold-formed steel pallet racking cross-sections for flexural–torsional buckling with constraints on the geometry, *Engineering Structures*, 31 (2009) 2711-2722.

- [24] AISI S100-12, American Iron and Steel Institute (AISI), North American specification for the design of cold-formed steel structural members, (2012).
- [25] J. Ye, I. Hajirasouliha, J. Becque, K. Pilakoutas, Development of more efficient cold-formed steel channel sections in bending, *Thin-Walled Structures*, 101 (2016) 1-13.
- [26] CEN, Eurocode 3: design of steel structures, part 1.3: general rules—supplementary rules for cold formed members and sheeting, in, Brussels: European Committee for Standardization, (2005).
- [27] D.T. Phan, J.B.P. Lim, T.T. Tanyimboh, W. Sha, An efficient genetic algorithm for the design optimization of cold-formed steel portal frame buildings, *Steel and Composite Structures, An International Journal*, 15(5) (2013) 519-538.
- [28] CEN, Eurocode 3: Design of Steel Structures, part 1-5: Plated structural elements, in, Brussels: European Committee for Standardization, 2005.
- [29] CEN, Eurocode 3: Design of Steel Structures. Part 1-1: General Rules and Rules for Buildings, in, Brussels: European Committee for Standardization, (2005).
- [30] ABAQUS, in, Hibbitt, Karlsson & Sorensen, Inc, Pawtucket, USA, 2007.
- [31] A.G.J. Way, R.M. Lawson, Design and installation of light steel external wall systems, *SCI Guide ED-017*, (2013).
- [32] O.K. Erol, I. Eksin, A new optimization method: Big Bang–Big Crunch, *Advances in Engineering Software*, 37 (2006) 106-111.
- [33] A. Kaveh, S. Talatahari, Size optimization of space trusses using Big Bang–Big Crunch algorithm, *Computers & Structures*, 87 (2009) 1129-1140.
- [34] O. Hasançebi, S. Kazemzadeh Azad, An exponential big bang-big crunch algorithm for discrete design optimization of steel frames, *Computers & Structures*, 110-111 (2012) 167-179.
- [35] D. Prayogo, M.-Y. Cheng, Y.-W. Wu, A.A. Herdany, H. Prayogo, Differential Big Bang - Big Crunch algorithm for construction-engineering design optimization, *Automation in Construction*, 85 (2018) 290-304.
- [36] Mathworks, Matlab R2011a, in, Mathworks, Inc, 2011.
- [37] CEN, Eurocode 0: “Basis of structural design.” , European Committee for Standardization, Brussels, (2002).
- [38] J. Becque, J.R. Rasmussen Kim, Numerical Investigation of the Interaction of Local and Overall Buckling of Stainless Steel I-Columns, *Journal of Structural Engineering*, 135 (2009) 1349-1356.

- [39] J. Becque, K.J.R. Rasmussen, A numerical investigation of local–overall interaction buckling of stainless steel lipped channel columns, *Journal of Constructional Steel Research*, 65 (2009) 1685-1693.
- [40] C. Yu, B.W. Schafer, Simulation of cold-formed steel beams in local and distortional buckling with applications to the direct strength method, *Journal of Constructional Steel Research*, 63 (2007) 581-590.
- [41] M.R. Haidarali, D.A. Nethercot, Finite element modelling of cold-formed steel beams under local buckling or combined local/distortional buckling, *Thin Wall Struct*, 49 (2011) 1554-1562.
- [42] L. Gardner, M. Ashraf, Structural design for non-linear metallic materials, *Eng Struct*, 28 (2006) 926-934.
- [43] B.W. Schafer, T. Peköz, Computational modeling of cold-formed steel: characterizing geometric imperfections and residual stresses, *Journal of Constructional Steel Research*, 47 (1998) 193-210.
- [44] S.M. Mojtabaei, M.Z. Kabir, I. Hajirasouliha, M. Kargar, Analytical and experimental study on the seismic performance of cold-formed steel frames, *Journal of Constructional Steel Research*, 143 (2018) 18-31.